Theory of collision-induced translation-rotation spectra: H 2 -He

PHYSICAL REVIEW A VOLUME 29, NUMBER 2 FEBRUARY 1984

Theory of collision-induced translation-rotation spectra: H_2-He

George Birnbaum
National Bureau of Standards, Washington, D.C. 20234

Shih-I Chu
Department of Chemistry, University of Kansas, Lawrence, Kansas 66045

A. Dalgarno
Harvard-Smithsonian Center for Astrophysics, Cambridge, Massachusetts 02138

Lothar Frommhold
Physics Department, University of Texas, Austin, Texas 78712

E. L. Wright
Department of Astronomy, University of California at Los Angeles, Los Angeles, California 90024
(Received 28 June 1983)

An adiabatic quantal theory of spectral line shapes in collision-induced absorption and emission is presented which incorporates the induced translation-rotation and translation-vibration spectra. The generalization to account for the anisotropy of the scattering potential is given. Calculations are carried out of the collision-induced absorption spectra of He in collisions with H_2 with *ab initio* electric dipole functions and realistic potentials. The anisotropy of the interaction potential is small and is not included in the calculations. The predicted spectra are in satisfactory agreement with experimental data though some deviations occur which may be significant. The rotational line shapes have exponential wings and are not Lorentzian. The connection between the quantal and classical theories is written out explicitly for the isotropic overlap induction.

I. INTRODUCTION

In a collision between two dissimilar atomic systems, overlap forces induce an electric dipole which gives rise to a translational spectrum in the far infrared (FIR). If one of the colliding pair is a nonpolar molecule, a dipole is produced by the electric fields of its multipole moments which polarize the partner. In addition to the multipole component of the induced dipole, there is an overlap component (usually weaker) and both give rise to translation-rotation absorption bands forbidden in the individual molecule. The spectra arise from free-free transitions, coupled with molecular transitions, in which the energy and momentum of the absorbed photon are transferred to the collisional atom-molecule pair.[1,2] Because induced dipoles exist only for times τ of the order of the duration of the collision, the spectra show a substantial bandwidth $\sim\tau^{-1}$, orders of magnitude greater than ordinary Doppler or pressure broadening. Emission and absorption due to the induced dipoles in collisions of neutral particles are much weaker than the familiar bremsstrahlung spectra of electrons, and collision-induced emission has only recently been observed in the laboratory.[3]

Apart from the general interest in collisional interactions which can be studied by collision-induced absorption (CIA) in novel ways, CIA is of astrophysical significance in regions of relatively high pressure and low temperature where ionization is weak. Trafton[4] has pointed out that the opacity of the atmospheres of the outer planets is largely due to H_2-H_2 and H_2-He collisions. The substantial enhancement of induced absorption due to H_2-He collisions[5,6] offers an interesting possibility for determining the H_2 to He ratio[7] in dense, cold regions of space. Collision-induced emission is significant in the atmospheres of cool stars.[8]

Whereas the FIR collision-induced absorption spectra of pure H_2 are well known from measurements at various temperatures and over extended frequency regions,[5,6,9–12] the spectra due to H_2-He collisions are less certain.[6] Because of the significance of the H_2-He absorption spectra, these are computed here from first principles to provide new information concerning the shape of these spectra and their variation with temperature.

Trafton[4,13] has given an adiabatic description of the translational absorption spectrum of a gas of pure H_2 and a gas mixture of H_2 and He. By comparing line shapes calculated with the assumption of an isotropic Lennard-Jones interaction potential with experimental spectra,[6] he obtained empirical parameters defining a simple analytical representation of the induced electric dipole. Wright and Dalgarno[14] calculated the induced electric dipole for H_2-He from the wave functions of Gordon and Secrest[15] and resolved it into three symmetry components. They calculated the adiabatic line shape of the translation-rotation spectra and obtained satisfactory agreement with measurement[5] by scaling the theoretical dipole moment by a factor

of 1.35. Recent calculations[16,17] show that the dipole moment of Wright and Dalgarno was not in error by such a large factor. Instead, the discrepancy may be attributed to the choice of the interaction potential. Collision-induced absorption spectra are sensitive to the region of the interaction potential when it passes through zero. Improved H_2-He interaction potentials[18–20] show that the zero of the potential adopted by Wright and Dalgarno[14] is located at too large a distance.

Based on improved H_2-He interaction potentials[18–20] and accurate computations of the induced dipole moment,[17] we undertake here a quantal calculation of the induced translation-rotation spectrum for comparison with the measurement. We present the theory for an anisotropic potential. The anisotropy of the H_2-He interaction is small, however, and the numerical calculations are based upon the isotropic component of the interaction. The spectra have three incoherent parts, one due to the isotropic component of the induced dipole, the others to anisotropic components. The computed spectra are tested by sum rules.[21–23] Although collision-induced vibration-rotation bands are not considered, the formalism can be generalized readily to include vibrational transitions.

II. THEORY OF THE LINE SHAPE

The absorption spectrum at temperature T and angular frequency $\omega=2\pi c\nu$ generated by collision-induced dipole moments can be written as[2,24]

$$\alpha(\omega)=\frac{4\pi^2}{3\hbar c}n_a n_b\omega(1-e^{-\beta\hbar\omega})Vg(\omega)\ , \tag{1}$$

where n_a and n_b are number densities of H_2 and He, $\beta=1/kT$, V is the volume, $\alpha(\omega)$ is expressed in cm^{-1}, and $g(\omega)$ is the spectral density. The product $Vg(\omega)$ is a function of the temperature T and depends upon specific molecular properties.[25] The spectral density is defined in terms of the matrix elements $\langle t\,|\,\vec{\mu}_{ss'}\,|\,t'\rangle$ of the electric dipole moment $\vec{\mu}$ by the formula

$$g(\omega)=\sum_{s,s'}P_s\sum_{t,t'}P_t\,|\,\langle t\,|\,\vec{\mu}_{ss'}\,|\,t'\rangle\,|^2\delta(\omega_{ss'}+\omega_{tt'}-\omega)\ , \tag{2}$$

where the subscript $s=\{v,j,m_j\}$ denotes the vibration-rotation states of the molecule, and $t=\{E_t$ or $k,l,m_l,J,M\}$ is an analogous vector designating the translational state of the collisional complex consisting of the molecule H_2 and atom He. Here l and m_l define the orbital angular momentum and its projection, and J and M are the coupled internal rotational and orbital angular momentum quantum numbers. A prime indicates a final state. Also, we have $\omega_{ss'}=(E_{s'}-E_s)/\hbar$ and $\omega_{tt'}=(E_{t'}-E_t)/\hbar$ which are molecular and translational transition frequencies, respectively, E_t is the energy of relative motion, and P_t is the normalized translational Boltzmann factor at the temperature T. It may be written

$$P_t=(\lambda_0^3/V)e^{-\beta E_t}\ , \tag{3}$$

where λ_0 is the de Broglie wavelength. This is given in terms of the reduced mass m of the collisional complex and temperature T by

$$\lambda_0^2=\hbar^2 2\pi\beta/m\ . \tag{4}$$

The molecular Boltzmann factor $P_s=P_vP_j$ designates a normalized population probability of a vibration-rotation state, where

$$P_j=g_j e^{-\beta E_j}\left[\sum_{j'}g_{j'}(2j'+1)e^{-\beta E_{j'}}\right]^{-1}\ . \tag{5}$$

For hydrogen, $g_j=1$ if j is even and $g_j=3$ if j is odd. At low temperatures, where vibration can be ignored, $P_{v=0}=1$ to a good approximation. The vibration-rotation matrix element of $\vec{\mu}$ in (2) is given by

$$\vec{\mu}_{ss'}=\langle s\,|\,\vec{\mu}(r\hat{r},R\hat{R})\,|\,s'\rangle\ , \tag{6}$$

where the vector $\vec{r}=r\hat{r}$ describes the orientation and separation of the hydrogen nuclei and $\vec{R}=R\hat{R}$ is the vector joining the centers of mass of the colliding atom and molecule.

If the induced dipole $\vec{\mu}$ has components μ_x and μ_y perpendicular to $\hat{R}$, and μ_z parallel to $\hat{R}$, the spherical components of the induced dipole can be expanded in the form[26,27]

$$\mu_\nu(r\hat{r},R\hat{R})=\frac{4\pi}{\sqrt{3}}\sum_{L\lambda}A_{L\lambda}(r,R)Y^{1\nu}_{\lambda L}(\hat{r},\hat{R})\ , \tag{7}$$

where $\mu_0=\mu_z$ and $\mu_{\pm1}=\mp(\mu_x\pm i\mu_y)/\sqrt{2}$. The interaction between H_2 and He consists mainly of the spherically symmetric component of the potential $V_0(R)$, and in our numerical calculations we ignored the orientation-dependent terms. By contrast, the dipole moment has strong orientation-dependent components. To take the orientation dependence of the dipole moment into account, we introduced in Eq. (7) the vector-coupled function $Y^{1\nu}_{\lambda L}$. These are eigenfunctions of the total angular momentum J and projection M, composed of the spherical harmonics $Y_{jm_j}(\hat{r})$ and $Y_{lm_l}(\hat{R})$, according to

$$Y^{JM}_{jl}(\hat{r},\hat{R})=\sum_{m_jm_l}C(j,l,J;m_j,m_l)Y_{jm_j}(\hat{r})Y_{lm_l}(\hat{R})\ , \tag{8}$$

where $M=m_j+m_l$ and $C(j_1,j_2,j_3;m_1,m_2)$ are Clebsch-Gordan coefficients.[28] A more general scattering theory of collision-induced absorption and emission is sketched in Appendix A. We calculate the matrix elements of (7) using the wave function of the collisional complex

$$\Psi^{JM}_{jlk}(r\hat{r},R\hat{R})=v_v(r)\frac{1}{R}u_{kl}(kR)Y^{JM}_{jl}(\hat{r},\hat{R})\ , \tag{9}$$

where we have assumed separability of vibrational, rotational, and translational motion. We have, furthermore, suppressed for convenience of notation the j dependence of the vibrational wave function $v_v(r)$. Using the Wigner-Eckart theorem[28] we may write for the angularly dependent part of the dipole matrix element

$$\langle j,l,J,M\,|\,Y^{1\nu}_{\lambda L}(\hat{r},\hat{R})\,|\,j',l',J',M'\rangle$$
$$=C(J,1,J';M,\nu)\langle j,l,J\,|\,|\,Y^1_{\lambda L}(\hat{r},\hat{R})\,|\,|\,j',l',J'\rangle\ . \tag{10}$$

Expressions for the reduced matrix element $\langle j,l,J\,|\,|\mu|\,|\,j',l',J'\rangle$ may be obtained for each component L,λ of (7) by multiplying (10) by $C(J,1,J';M,\nu)$ and summing over M,M',ν to give

$$\langle j,l,J \,||\, Y^1_{\lambda L} \,||\, j',l',J'\rangle = \frac{\sqrt{3}}{4\pi}[(2j+1)(2l+1)(2J+1)(2\lambda+1)(2L+1)]^{1/2} C(l,L,l';0,0)C(j,\lambda,j';0,0) \begin{Bmatrix} j' & l' & J' \\ j & l & J \\ \lambda & L & 1 \end{Bmatrix}, \tag{11}$$

where $\{\ \}$ is a 9-j symbol identical to Fano's $X(j',l,J';j,l,J;\lambda,L,1)$.[29]

The wave function $\mu_{kl}(kR)$ in (9) is the solution of the radial Schrödinger equation

$$\left[\frac{d^2}{dR^2}+k^2-\frac{l(l+1)}{R^2}-\frac{2m}{\hbar^2}V_0(R)\right]u_{kl}(kR)=0\ , \tag{12}$$

where $\hbar^2k^2=2mE_t$ and $V_0(R)$ is the spherical average of the interaction potential. The equation is solved subject to the boundary conditions

$$u_{kl}(kR)\rightarrow \begin{cases} 0, & \text{as } R\rightarrow 0 \\ \left(\dfrac{2m}{\pi\hbar^2k}\right)^{1/2}\sin(kR-\pi l/2+\delta_l)\ , & \end{cases} \tag{13}$$

$$\text{as } R\rightarrow\infty \tag{14}$$

where δ_l is the scattering phase shift. It is convenient to use the energy normalization

$$\int_0^\infty u_{kl}(kR)u_{k'l}(k'R)dR=\delta(E_{t'}-E_t)\ , \tag{15}$$

so that the sums over energy in (2) may be replaced by the integrals $\int\int\cdots dE\,dE'$.

The sum of squares of the matrix elements of dipole components (7) can be written

$$\sum_{M,M',\nu}|\langle i\,|\,\mu_\nu\,|\,f\rangle|^2 = (2J'+1)\left|\sum_{L,\lambda}\langle l,k\,|\,A_{L\lambda}(R)\,|\,l',k'\rangle\frac{4\pi}{\sqrt{3}} \times\langle j,l,J\,||\,Y^1_{\lambda L}\,||\,j',l',J'\rangle\right|^2, \tag{16}$$

where i,f signify the initial and final state, respectively, and

$$A_{L\lambda}(R)=\langle v\,|\,A_{L\lambda}(r,R)\,|\,v'\rangle \tag{17}$$

is the vibrational matrix element, which we specialize now to the case in which $v=v'=0$. Note that the square of the sums in (16) is the same as a multiple sum over L,λ and L',λ'. From (2) and (16) we get

$$g(\omega)=\hbar\sum_{j,j'}(2j+1)P_j \times\sum_{l,l'}\int_0^\infty dE_tP_t\sum_{JJ'}(2J'+1) \times\sum_{M,M',\nu}|\langle i\,|\,\mu_\nu\,|\,f\rangle|^2, \tag{18}$$

where we have already integrated over $E_{t'}$. The factor $\hbar$ stems from converting the δ function of frequency in (2) to one of energy. The δ function imposes the condition $\hbar\omega=(E_{t'}-E_t)+(E_{j'}-E_j)$ on the remaining integration in (18). Since the radial wave functions are independent of J and J', the matrix elements in Eq. (16) can be written as a product and summed over J and J' according to

$$\sum_{J,J'}(2J'+1)\langle j,l,J\,||\,Y^1_{\lambda L}\,||\,j',l',J'\rangle\langle j,l,J\,||\,Y^1_{\lambda'L'}\,||\,j',l',J'\rangle = \delta_{\lambda\lambda'}\delta_{LL'}\frac{3}{16\pi^2}(2j+1)(2l+1) \times[C(l,L,l';0,0)]^2[C(j,\lambda,j';0,0)]^2\ , \tag{19}$$

the cross products disappearing. Thus

$$Vg(\omega)=\lambda_0^3\hbar\sum_{L,\lambda}\sum_{j,j'}(2j+1)P_j[C(j,\lambda,j';0,0)]^2\sum_{l,l'}(2l+1)[C(l,L,l';0,0)]^2 \times\int_0^\infty|\langle l,k\,|\,A_{L\lambda}(R)\,|\,l',k'\rangle|^2e^{-\beta E_t}dE_t\ . \tag{20}$$

Energy conservation is imposed by the δ function in (2) which defines an upper state k' under the integral for any fixed k, j, j', and ω. The radial wave functions $u_{lk}(kR)/R$ and matrix elements must be obtained by numerical integration.

Equation (20) is of the form $g(\omega)=G_{10}(\omega)+G_{12}(\omega)+G_{32}(\omega)+\cdots$, each component $G_{L\lambda}(\omega)$ containing a translational contribution with $j'=j$ and a number of rotational lines with $j'\neq j$,

$$G_{L\lambda}(\omega)=\sum_j(2j+1)P_j[C(j,\lambda,j;0,0)]^2g_{L\lambda}(\omega)+\sum_{j\neq j'}(2j+1)P_j[C(j,\lambda,j';0,0)]^2g_{L\lambda}(\omega-\omega_{jj'})\ . \tag{21}$$

For fixed L,λ, the functions $g_{L\lambda}(\omega)$ are the same and are given by

$$Vg_{L\lambda}(\omega)=\lambda_0^3\hbar\sum_{l,l'}(2l+1)[C(l,L,l';0,0)]^2\int_0^\infty |\langle l,k\,|\,A_{L\lambda}(R)\,|\,l',k'\rangle|^2 e^{-\beta E_t}dE_t\ , \tag{22}$$

but shifted by the rotational frequencies $\omega_{jj'}$ (which will be negative if $j'<j$). From $G_{L\lambda}(R)$, the absorption coefficient $\alpha(\omega)$ is computed according to

$$\alpha(\omega)=\sum_{L,\lambda}\alpha_{L\lambda}(\omega)\ , \tag{23}$$

with

$$\alpha_{L\lambda}(\omega)=\frac{4\pi^2}{3\hbar c}n_a n_b\omega(1-e^{-\beta\hbar\omega})VG_{L\lambda}(\omega)\ . \tag{24}$$

Each $\alpha_{L\lambda}(\omega)$ features a translational component and a number of rotational lines just as $G_{L\lambda}$. The frequency-dependent factor $[1-\exp(-\beta\hbar\omega)]$ accounts for stimulated emission.

The computations to be presented below are based on numerical solutions of Eq. (22) for selected isotropic potentials. From the solutions, the radial matrix elements are computed and substituted into the translational spectral density (22) to yield rotation-translation spectra (21) and (24).

Moment relations[21–23] (sum rules) are used to test the computed results. Since translational and rotational profiles are given in terms of the same function $g_{L\lambda}(\omega)$, it is sufficient to consider the unshifted spectral function for each given L,λ. Their zeroth and first spectral moments G_0 and G_1 are given by[21,23]

$$G_0=V\int_{-\infty}^{\infty}g_{L\lambda}(\omega)d\omega=4\pi\int_0^\infty[A_{L\lambda}(R)]^2g(R)R^2dR\ , \tag{25}$$

$$G_1=V\int_{-\infty}^{\infty}\omega g_{L\lambda}(\omega)d\omega=\frac{2\pi\hbar}{m}\int_0^\infty\left[\left[\frac{dA_{L\lambda}}{dR}\right]^2+\frac{L(L+1)}{R^2}[A_{L\lambda}(R)]^2\right]g(R)R^2dR\ . \tag{26}$$

These are translational quantities which are not affected by the molecular state or transition. The function $g(R)$ is usually taken as the low-density limit of the classical radial distribution function, $g(R)=\exp[-\beta V_0(R)]$, with wave-mechanical corrections[23,30] to the order of h^2. This is sufficiently accurate for H_2-He at $T\geq 190$ K.

Collision-induced vibrational bands can also be obtained by evaluating the vibrational matrix elements (17). The molecular frequencies $\omega_{ss'}$ then must include vibrational transitions and the molecular Boltzmann factor must include vibrational states.

Although the theory is developed for the atom-diatom pair, it also describes the essential features of the diatom-diatom (H_2-H_2) collision-induced spectra. The atom is formally replaced by the spherical average of the second diatom which is assumed to be without internal structure. While simultaneous transitions in both collisional partners cannot be described in this formulation, they are known from experiment to be extremely weak and can be ignored in a first approximation. An accurate description of the H_2-H_2 translation-rotation spectra based on (20) may be obtained as suggested by preliminary computations.[31]

Specialization of the results obtained here to the interaction of dissimilar atoms is straightforward. In such cases, the induced dipole (7) consists solely of the term $L=1,\lambda=0$, and rotational excitation is not possible. The resulting translational spectrum is given by (22) and (24), with the two nonvanishing coefficients $(2l+1)[C(l,1,l+1;0,0)]^2=l+1$, and $(2l+1)[C(l,1,l-1;0,0)]^2=l$. The resulting expressions are in agreement with previous work.[32,33] It can be shown similarly that collision-induced light scattering by pairs of atoms results in a spectral function (22), with the induced dipole operator replaced by diatom polarizability invariants, and $L=0$ and 2.[34]

III. DETAILS OF THE LINE-SHAPE COMPUTATIONS

Adiabatic line shapes (22) can be obtained if the isotropic part of the interaction potential is known, along with the induced components $A_{L\lambda}(R)$. We use a computer code which is an extension of an existing program developed originally for collision-induced light scattering[34] and absorption.[33] The spectral functions $Vg_{L\lambda}(\omega)$ are obtained at 15 different frequencies (i.e., 0, 3, 8, 20, 40, 70, 100, 140, 200, 280, 400, 560, 800, 1000, and 1200 cm^{-1}). A third-order spline interpolation of the logarithm of $g_{L\lambda}(\omega)$ is employed, followed by exponentiation, to compute the spectral function at positive frequencies. Logarithmic interpolation proved to be more accurate than direct interpolation. A straightforward exponential extrapolation is used at the high frequencies, which, however, has little effect on the zeroth and first moments, or on the appearance of the spectra. To compute $g(\omega)$ at negative frequencies, we use detailed balance

$$g_{L\lambda}(-\omega)=e^{-\beta\hbar\omega}g_{L\lambda}(\omega)\ . \tag{27}$$

Sample computations at negative frequencies were seen to be consistent with (27). For each computed line shape, zeroth and first moments are obtained by integration of the spectral intensity and compared with the sum rules (25) and (26), and are typically found to be in agreement to within $\sim 2\%$. Higher precision has been obtained in trial runs at the expense of increased computer time.

At room temperature, about thirty partial waves contribute to the H_2-He spectrum. Computations of the 60 000 matrix elements needed for a line shape at 300 K, based on three induced parts $L,\lambda=1,0$, 3,2, and 1,2, require about 2000 sec of CPU (central processor unit) time on a Control Data Corporation Cyber-750/150 computer. Line

shapes are computed from the recorded matrix elements for a variety of temperatures in seconds.

A. Induced Dipole

The induced dipole components $A_{L\lambda}$ have been computed from first principles.[14,16,17] We base our computations on the recent work of Wormer and van Dijk[17] which shows that for $L=\lambda+1$ the induced dipoles are of the form

$$A_{L\lambda}(R)=\mu_{L\lambda}e^{-R/\rho_{L\lambda}}+C_n/R^n . \tag{28}$$

For the isotropic component ($L=1$),[17] the induced dipole components are

$$\mu_{10}=25.019$$

in a.u. and (29)

$$\rho_{10}=0.6115a_0 .$$

The leading dispersion term is $C_7=-61.8$ a.u.[16] For the quadrupole-induced dipole, the constants are given by[17]

$$\mu_{32}=-0.3224$$

in a.u. and (30)

$$\rho_{32}=0.8190a_0 ,$$

$$C_4=\sqrt{3}\alpha\theta=1.16 \tag{31}$$

in a.u. The helium polarizability α is given in Ref. 35 and the hydrogen quadrupole moment θ in Ref. 36.

The other nonvanishing coefficients of the induced dipole are those with $L=\lambda-1$ which are purely short range. Except for A_{12}, given by

$$A_{12}(R)=-(35.361\times10^{-5})\exp\left[\frac{(\sigma_0-R)}{0.56075a_0}-\frac{(\sigma_0-R)^2}{5.8211a_0^2}\right] \tag{32}$$

in a.u., with $\sigma_0=5.742a_0$, they are not significant.

Other components ($L=5,\lambda=4$ and $L=5,\lambda=6$) have been determined.[17] However, the associated spectral intensities amount to only a few hundredths of one percent of the total intensity, owing to the smallness of high-order overlap dipoles[17] and the higher multipole moments,[36–38] and we ignore them.

B. Potential

Previously, a Lennard-Jones 6-12 potential with $\sigma=2.75$ Å and $\epsilon/k=19.7$ K (Ref. 39) has been used for analyzing collision-induced absorption in He-H_2. Recent theoretical work[19,20,40–48] has resulted in much improved potentials with significantly larger collision diameters σ of $\simeq$3.0 Å. Empirical potentials based on nuclear magnetic resonance[49,50] and transport data[51] have been proposed. That by Gengenbach and Hahn,[18] which is based on molecular beam scattering over a range of energies up to 2.9 eV is probably the most reliable in the vicinity of the collision diameter which is so important for CIA intensities. Shafer and Gordon adopted it to determine an empirical anisotropy.[52] Detailed discussions of the various He-H_2 potentials can be found elsewhere.[19,20,52] For our computations of the absorption spectra we chose the empirical[18] and *ab initio*[20] potentials as representative examples of the H_2-He interaction.

IV. RESULTS

A. Calculated *ab initio* absorption spectra

The spectra consist of a broad pure translational part, dominated by the isotropic component ($L=1,\lambda=0$, marked 1-0 in Figs. 1–3), and generally smaller contributions from the anisotropic components (marked 3-2 and 1-2, respectively). The rotational lines are due to the quadrupole induction (3-2), and a weaker quadrupolar overlap contribution from the 1-2 component.

At the high temperatures, the two potentials lead to spectra which are in reasonable agreement. At the lowest temperature (77 K), differences of 15% occur in the translational part, but the rotational-line intensities are apparently not affected by the small differences of the potentials. The rotational-line intensities are dominated by the long-range quadrupolar induction term C_4/R^4. Line spectra based on this induction mechanism effectively average potentials over a relatively large range of distance which often reduces the effects of differences between potential models. The isotropic part, in contrast, has a much shorter range owing to the small ρ_{10} and has an almost negligible dispersion part. The translational profile, which is basically due to this induction mechanism, magnifies the differences of the potentials over a very small range of separations near their collision diameters, which, however, in the present case differ by only 1.3%.

Theoretical potentials tend to overestimate[53] the magnitude of σ and, indeed, the *ab initio* value[20] of σ is $5.745a_0$,

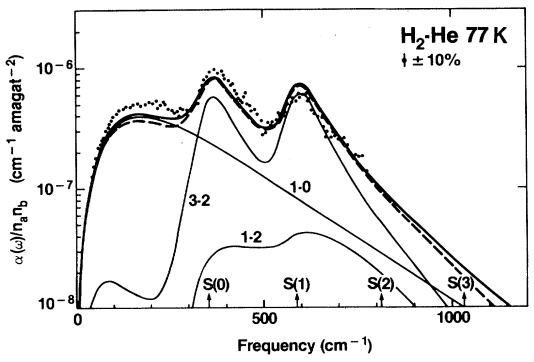

FIG. 1. Absorption spectrum at 77.4 K due to H_2-He collisions. The heavy line represents the total theoretical intensities given by the sum of the three components shown as light curves marked L-λ=1-0, 1-2, and 3-2. The computation is based on the *ab initio* induced dipole (28-32) and the empirical potential of Gengenbach and Hahn (Ref. 18). The dashed curve is, similarly, the total computed intensity, but based instead on an *ab initio* potential of Meyer *et al.* (Ref. 20). The dots are measurements by Birnbaum (Ref. 6). The arrows indicate the rotational-line positions of hydrogen.

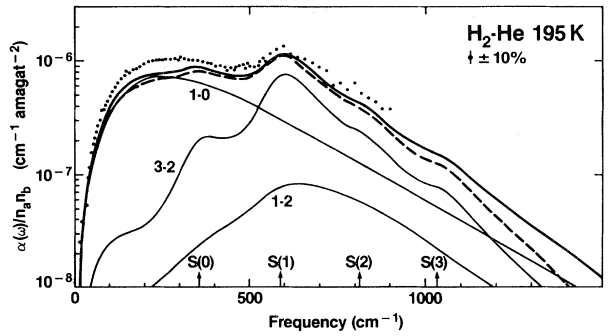

FIG. 2. Absorption spectrum at 195 K due to H_2-He collisions. Details are as for Fig. 1.

compared to the empirical value[18] of $5.671a_0$. A collision diameter too large by 1% produces an intensity deficiency of about 10% in the case of short-range induction. The longer-ranged inductions usually show a lesser sensitivity to σ. Our preference is for the spectra based on the empirical potential.[18]

B. Moments

Zeroth and first spectral moments may be calculated from the profiles using the left-hand sides of Eqs. (25) and (26). The results for 77, 195, and 297 K are given in the columns labeled $g(\omega)$ in Table I. The moments can also be obtained directly from the interaction potential and induced-dipole component, without computing the spectral function, by using the right-hand sides of (25) and (26). These results are given for $T=195$ and 297 K in columns marked $\sum$ in Table I. The former are exact wave-mechanical values, while the latter are based on a classical expression of the pair distribution function with wave-mechanical corrections to the order $\sim h^2$. Comparisons are carried out for several contributions of the dipole moment and potential functions. For the isotropic components, the lowest-order quantal corrections amount to $\sim 10\%$ at 297 K, $\sim 15\%$ at 195 K, and 30—40 % at 77 K. Whereas at the two highest temperatures the corrections reduce the error to an acceptable limit of 2%, at 77 K a much greater error occurs and the present sum rules with lowest-order quantum corrections are less useful. (Sum-rule moments are, therefore, not given in Table I for the lowest temperature.) For the quadrupole-induced part, the lowest-order quantum corrections are smaller and often negative. Apparently, the long-range nature of the quadrupole-induced dipole is associated with substantial positive corrections at small distances, and negative corrections at large distances and these corrections tend to cancel. The small anisotropic component with $L=1,\lambda=2$ shows the same short-range behavior as the isotropic part, with quantal corrections that are large and positive.

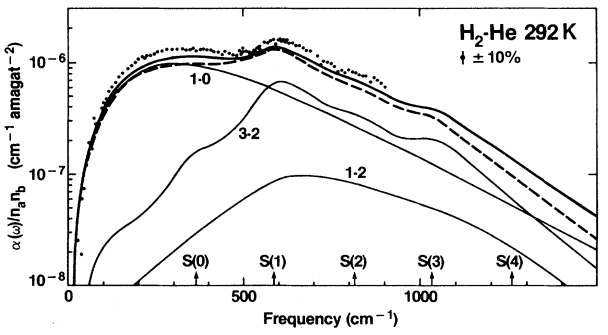

FIG. 3. Absorption spectrum at 292.4 K due to H_2-He collisions. Details are as for Fig. 1.

At 297 K the moments based on the spectral function and sum rules agree within 1—3 %, the sum rules giving the greater values. The agreement is within the uncertainty of the line-shape computation and confirms the correctness of the computed spectra. Quantal corrections are significant for the H_2-He system even at 300 K.

C. Comparison with experiment

The measurements of $\alpha(\omega)$ are shown as dots in Figs. 1—3. They lie consistently above theory by as much as 20% except for the strong $S_0(1)$ line at 77 K, where the measured absorption is less than the computed value. The H_2-He spectra are obtained by subtracting two comparable measurements, one in the mixture and the other in pure hydrogen. Consequently, the difference spectra for H_2-He collisions is of lower accuracy than for neat systems. However, since the most prominent difference of the H_2-He spectrum from the H_2-H_2 spectrum is the translational component generated by the isotropic part of the induced dipole, a feature which is absent in pure hydrogen, errors should be relatively small in the measurement of the translational spectrum of the mixture. The rotational lines, on the other hand, are in order of magnitude more intense in pure hydrogen at comparable densities, so that the measurements of the rotational lines in the mixture are of lesser accuracy even when optimal mixture ratios are employed.

With the help of a model line-shape function[54] and a least-mean-squares fitting procedure it is possible to decompose the measured spectra[6] into approximate isotropic and anisotropic components.[55] The empirical isotropic line shape can be compared with the computed spectral function $g_{10}(\omega)$. The model line shape is more intense than the calculated line shape particularly at lower temperatures and falls off faster than the theoretical profiles, suggesting a slightly longer range ρ_{10} for the induced isotropic dipole than that given in Eq. (29).

We were led to a similar conclusion from an empirical determination of the range parameter $\rho=0.337$ Å, a value which is nearly unaffected by the uncertainties of the interaction potentials.[55] However, the falloff of the model line shape is even steeper than this empirical range would suggest. Thus the *ab initio* range ρ_{10} is probably too small.

D. Uncertainty of computed spectra

The comparison of moments computed from the quantum line shape and from sum rules at the higher tempera-

TABLE I. Computed spectral moments of H_2-He absorption spectra compared for various induced models, $A_{L\lambda}$, and isotropic interaction potentials, labeled by the equation (in parentheses) or reference number. $g(\omega)$ signifies the moments G_0 and G_1 obtained by integrating spectral density profiles, and $\sum$ indicates moments obtained from the sum rules, Eqs. (25) and (26).

$A_{L\lambda}$ (Eq.) or Ref.	$V(R)$ Ref.	$T=77$ K $10^{62}G_0$ erg cm^6 $g(\omega)$	$T=77$ K $10^{49}G_1$ erg cm^6/s $g(\omega)$	$T=195$ K $10^{62}G_0$ erg cm^6 $g(\omega)$	$\sum$	$T=195$ K $10^{49}G_1$ erg cm^6/s $g(\omega)$	$\sum$	$T=297$ K $10^{62}G_0$ erg cm^6 $g(\omega)$	$\sum$	$T=297$ K $10^{49}G_1$ erg cm^6/s $g(\omega)$	$\sum$
$L=1,\lambda=0$											
(29)	18	0.397	0.969	0.944	0.973	2.27	2.34	1.51	1.55	3.59	3.70
(29)	20	0.362	0.884	0.829	0.850	1.99	2.05	1.37	1.41	3.27	3.37
16	20	0.352	0.962	0.849	0.870	2.28	2.34	1.46	1.50	3.89	4.02
16	19	0.349	0.951	0.878	0.907	2.36	2.44	1.44	1.48	3.84	3.97
16	45	0.529	1.44	1.24	1.28	3.32	3.44	1.96	2.02	5.22	5.39
16	39	0.751	2.04	1.40	1.45	3.74	3.89	1.95	2.01	5.16	5.38
$L=1,\lambda=2$											
(32)	18	0.014	0.030	0.031	0.032	0.061	0.062	0.047	0.048	0.087	0.088
(32)	20	0.013	0.029	0.028	0.028	0.055	0.056	0.043	0.044	0.079	0.081
$L=3,\lambda=2$											
(30),(31)	18	0.136	0.116	0.198	0.201	0.190	0.193	0.024	0.025	0.251	0.256
(30),(31)	20	0.133	0.111	0.188	0.191	0.177	0.179	0.023	0.024	0.234	0.239
(31)	20	0.086	0.057	0.114	0.115	0.085	0.086	0.013	0.014	0.108	0.110
(31)	19	0.084	0.056	0.114	0.116	0.086	0.087	0.013	0.014	0.108	0.111
(31)	45	0.098	0.069	0.130	0.133	0.103	0.105	0.015	0.016	0.128	0.132
(31)	39	0.116	0.087	0.144	0.146	0.116	0.118	0.016	0.016	0.136	0.139

tures indicates a *precision* of the line-shape calculations of better than 2%. This precision is nearly uniform over the frequency range considered, and only in the far wings of the spectral function $g(\omega)$, where the intensities have fallen off to less than 10^{-3} of the peak value, do the numerical inaccuracies increase.[33,34] This does not significantly affect the precision of the computed absorption spectra shown in Figs. 1–3.

The *accuracy* of the computed line shapes is controlled by the input functions. The calculated and measured line shapes of the translational spectra differ somewhat as Figs. 1–3 illustrate. At the higher temperatures, the difference in the peak translational intensities of between 10% and 15% may exceed the experimental uncertainties and be significant. At 77 K the differences amount to about 25% and probably are outside the errors of the measurement. The observed differences are due presumably to uncertainties in the potential, to approximations such as the neglect of electron correlation in the calculation of the induction models, and to measurement error. The failure to account for the anisotropy of the potential is not likely to lead to an error which is significant compared with the experimental error.

The uncertainty of present potential models amounts to a 10% change for the isotropic and a smaller change for the anisotropic components. This is illustrated in the figures by the solid and dashed lines, where computed spectra based on different potentials[18,20] are compared. Table I compares the computed spectral moments which show the same tendencies, lines 2 and 3 for the isotropic part, and lines 7 and 8, and 9 and 10 for the anisotropic components. Earlier potential models like the HFD model[45] give rise to substantial uncertainties, from 30% to 50%, if comparable induced dipoles are input as shown by lines 3 and 5 of Table I. The unsuitability of a Lennard-Jones potential[13,39] is seen by comparing lines 3 and 6 of Table I.

An estimate of the effect of uncertainties associated with the *ab initio* induced dipoles can be obtained in similar ways. Berns *et al.*[16] used a variational approach to calculate induced-dipole components. Spectral moments computed with their isotropic induced component differ by almost 20% at high temperatures; compare lines 2 and 3 of Table I. The main anisotropic component is even more uncertain as the comparison of lines 10 and 11 shows. We note that Berns *et al.* do not obtain an anisotropic overlap contribution, the quadrupole induction consisting of the R^{-4} term only. Recent preliminary results by Meyer[56] apparently support the results of Wormer and van Dijk[17] at the separations of interest. The agreement is at the 5% level which indicates an uncertainty of 10% for the computed spectra, because of the quadratic dependence on the dipole strength.

V. CONCLUSION

We have formulated a wave-mechanical theory of the line shape of collision-induced absorption in the adiabatic approximation. The theory is applicable to the translation-rotation spectra of collisional systems consisting of an atom and a diatomic molecule. It was used to compute CIA spectra of H_2-He, for which accurate dipole functions and interaction potentials are available. The ro-

tational line shapes, which are computed here for the first time on the basis of a rigorous theory, show exponential wings and are not Lorentzian as previously assumed.[1]

While we have not considered vibrational CIA spectra, the formalism is applicable directly to that case. It can also be used to calculate the line shapes of pairs of colliding diatomic molecules.

For reliable predictions of CIA intensities, accurate values of the repulsive interaction for separations near the collision diameter must be used. The exceedingly strong dependence of CIA spectra, particularly the isotropic and other short-range parts, on the repulsive interaction suggests that it may be interesting to test the assumption regarding the neglect of anisotropy.

ACKNOWLEDGMENTS

The work of A. Dalgarno was supported in part by the National Science Foundation under Grant No. AST-81-14718. The work of G. Birnbaum was supported in part by a contract from the Jet Propulsion Laboratory, sponsored by the Planetary Atmospheres Program, National Aeronautics and Space Administration.

APPENDIX A: EFFECT OF ANISOTROPIC POTENTIAL

To take into account the anisotropy of the interaction potential we introduce wave functions[57] according to

$$\Psi^{JM}_{jlk}(R\hat{R},\hat{r})=\sum_{j'}\sum_{l'}R^{jlJ}_{j'l'k}(R)Y^{JM}_{j'l'}(\hat{R},\hat{r})/R\ , \tag{A1}$$

where the radial wave functions are regular at the origin, satisfy the coupled Schrödinger equation given by Arthurs and Dalgarno,[57] and behave asymptotically as

$$R^{jlJ}_{j'l'k}(R)=\left[\frac{2m}{\pi\hbar^2k}\right]^{1/2}F^{-1/2}\left[\delta_{jj'}\delta_{ll'}\sin(kR-l\pi/2)-\left[\frac{k}{k'}\right]^{1/2}R^J(j,l;j',l')\cos(k'R-l'\pi/2)\right] \tag{A2}$$

in which the wave numbers k' and k are related by

$$\frac{\hbar^2}{2m}k^2+E_j=\frac{\hbar^2}{2m}k'^2+E_{j'}\ . \tag{A3}$$

The matrix R is defined by $R=i(1+S)^{-1}(1-S)$, where S is the scattering matrix and the factor

$$F=1+\sum_{j',l'}[R^J(j,l;j',l')]^2 \tag{A4}$$

normalizes the flux of incoming particles.

The collision-induced absorption coefficient is obtained by inserting the extra sums over exit channels into Eq. (22). The closed-form sum over J and J' cannot be used, as the radial wave functions depend on J. The radial matrix elements are given by

$$\langle j,l,J,k;j_2,l_2\,|\,A_{L\lambda}\,|\,j',l',J',k';j_3,l_3\rangle = \int R^{jlJ}_{j_2l_2k}(R)A_{L\lambda}(R)R^{j'l'J'}_{j_3l_3k'}(R)dR\ . \tag{A5}$$

The collision-induced absorption coefficient becomes

$$\alpha(\omega)=\frac{4\pi^2}{3c}\lambda_0^3n_an_b\omega(1-e^{-\beta\hbar\omega})\times\sum_{j,j'}P_j\int dE_te^{-\beta E_t}\sum_{l,l'}\sum_{J,J'}(2J'+1)\times\left|\sum_i\sum_{j_2}\sum_{l_2}\sum_{j_3}\sum_{l_3}\langle j_2,l_2,J\,||\,Y^1_{\lambda L}\,||\,j_3,l_3,J'\rangle\langle j,l,J,k;j_2,l_2\,|\,A_{L\lambda}\,|\,j',l',J',k';j_3,l_3\rangle\right|^2\ . \tag{A6}$$

APPENDIX B: THE CLASSICAL LIMIT—SPHERICAL CASE

It is instructive to make the detailed connection between the classical and quantal expressions for the absorption coefficient. To avoid the complexities of angular momentum coupling, we consider the case of a pair of colliding atoms for which the summation over partial waves in Eq. (20) reduces to the form

$$\sum_{l'=l\pm1}\sum_{l}l'\,|\,\langle l,k\,|\,\mu(R)\,|\,l',k'\rangle\,|^2\ . \tag{B1}$$

For the radial wave functions, we use the WKBJ approximations

$$u_{Lk}(R)=\left[\frac{2m}{\pi\hbar^2k}\right]^{1/2}\sin\left[\int_{R_c}^{R}k(r)dr\right]\ , \tag{B2}$$

where

$$k(R)=\frac{1}{\hbar}\left[2m\left[E_t-\frac{L^2}{2mR^2}-V_0(R)\right]\right]^{1/2}\ . \tag{B3}$$

R_c is the classical distance of closest approach and $L^2=\hbar^2l(l+1)$ is the square of the orbital angular momentum. In the final state, $l=l\pm1$ and

$$k'(R)=\frac{1}{\hbar}\left[2m\left[E_t+\hbar\omega-\frac{(L\pm\hbar)^2}{2mR^2}-V_0(R)\right]\right]^{1/2}\ . \tag{B4}$$

In the classical limit as $\hbar\to0$, the oscillations in the WKBJ wave functions become infinitely rapid but the difference in phase between $u_{lk}(R)$ and $u_{l'k'}(R)$ remains finite. Thus

$$\lim_{\hbar\to0}[k'(R)-k(R)]=\frac{m}{\hbar k(R)}\left[\omega\mp\frac{L}{mR^2}\right]\ . \tag{B5}$$

Using the formula

$$\sin x \sin y = \tfrac{1}{2}[\cos(x-y)-\cos(x+y)]$$

and neglecting the second rapidly oscillating term, we obtain for the matrix-element limit

$$\lim_{\hbar\to 0}\langle LE\,|\,\mu\,|\,L\pm\hbar,E+\hbar\omega\rangle = \frac{m}{\pi\hbar^2 k}\int_0^\infty \mu(R)dR \times \int_{R_c}^R \cos\left[\frac{m}{\hbar k(r)}\left[\omega\mp\frac{L}{mr^2}\right]\right]dr \ . \quad \text{(B6)}$$

If we introduce the variables

$$\theta = \mp\int_0^t \frac{L}{mr^2}dt \ , \qquad t = \pm\int_{R_c}^R \frac{m}{\hbar k(r)}dr \ , \quad \text{(B7)}$$

the limit may be written in the form

$$\lim_{\hbar\to 0}\langle LE\,|\,\mu\,|\,L\pm\hbar,E+\hbar\omega\rangle = \frac{1}{2\pi\hbar}\int_{-\infty}^{\infty}\mu(t)e^{i\theta}e^{i\omega t}dt \ , \quad \text{(B8)}$$

so that the matrix elements are the Fourier transform of the classical dipole.

If the number of contributing partial waves is large, we may replace the discrete summation over l by an integration. The angular momentum is related to the impact parameter b according to $L=l\hbar=kb\hbar$. Thus

$$\sum_{l'=l\pm1}\sum_{l} l'\,|\,\langle l,k\,|\,\mu(R)\,|\,l',k'\rangle\,|^2 \approx \frac{k^2}{2\pi^2\hbar^2}\int b\left|\int_{-\infty}^{\infty}\mu(t)e^{i\omega t}dt\right|^2 db = \frac{mE_t}{\pi^2\hbar^4}\int b\left|\int_{-\infty}^{\infty}\mu(t)e^{i\omega t}dt\right|^2 db \ . \quad \text{(B9)}$$

Finally carrying out the integration over E_t in (20), we obtain the classical formula appropriate for $\hbar\omega \ll k_B T$ (Ref. 58):

$$\alpha(\omega) = \frac{4(2\pi)^{3/2}}{3c(mk_BT)^{1/2}}n_a n_b\omega^2\int db\, b\int dx\, x\, e^{-x}\left|\int_{-\infty}^{\infty}\mu(t)e^{i\omega t}dt\right|^2 , \quad \text{(B10)}$$

where $x=E_T/kT$.

[1]H. L. Welsh, Int. Rev. Sci., Phys. Chem. Ser., Spectrosc. 3, 33 (1972).

[2]G. Birnbaum, B. Guillot, and S. Bratos, Adv. Chem. Phys. 51, 49 (1982).

[3]R. Krech, G. Caledonia, S. Schertzer, K. Ritter, T. Wilkerson, L. Cotnoir, R. Taylor, and G. Birnbaum, Phys. Rev. Lett. 49, 1913 (1982).

[4]L. M. Trafton, Astrophys. J. 146, 558 (1966); 147, 765 (1967).

[5]Z. J. Kiss, H. P. Gush, and H. L. Welsh, Can. J. Phys. 37, 362 (1959).

[6]G. Birnbaum, J. Quant. Spectrosc. Radiat. Transfer 19, 51 (1978).

[7]Th. Encrenaz, D. Gautier, L. Vapillon, and J. P. Verdet, Astron. Astrophys. 11, 431 (1971); D. Gautier, B. Conrath, M. Flaser, R. Hanel, V. Kunde, A. Chedin, and N. Scott, J. Geophys. Res. 86, 8713 (1981).

[8]J. Linsky, Astrophys. J. 156, 989 (1969).

[9]J. P. Colpa and J. A. A. Ketelaar, Mol. Phys. 1, 14 (1958).

[10]D. R. Bosomworth and H. P. Gush, Can. J. Phys. 43, 729 (1965).

[11]J. W. MacTaggart and J. L. Hunt, Can. J. Phys. 47, 65 (1969).

[12]S. Cunsolo and H. P. Gush, Can. J. Phys. 50, 2058 (1972).

[13]L. Trafton, Astrophys. J. 179, 971 (1973).

[14]E. L. Wright and A. Dalgarno (unpublished).

[15]R. G. Gordon and D. Secrest, J. Chem. Phys. 52, 120 (1970).

[16]R. M. Berns, P. E. S. Wormer, F. Mulder, and A. van der Avoird, J. Chem. Phys. 69, 2102 (1978).

[17]P. E. S. Wormer and G. van Dijk, J. Chem. Phys. 70, 5695 (1979).

[18]R. Gengenbach and C. Hahn, Chem. Phys. Lett. 15, 604 (1972).

[19]F. Mulder, A. van der Avoird, and P. E. S. Wormer, Mol. Phys. 37, 159 (1979).

[20]W. Meyer, P. C. Hariharan, and W. Kutzelnigg, J. Chem. Phys. 73, 1880 (1980).

[21]J. van Kranendonk and Z. Kiss, Can. J. Phys. 37, 1187 (1959).

[22]J. P. Colpa and J. A. A. Ketelaar, Mol. Phys. 1, 343 (1958).

[23]J. D. Poll and J. L. Hunt, Can. J. Phys. 54, 461 (1976).

[24]M. S. Miller, D. A. McQuarrie, G. Birnbaum, and J. D. Poll, J. Chem. Phys. 57, 618 (1972).

[25]We note that in other works on the subject the reciprocal volume of (3) is often absorbed by replacing P_t by VP_t in the definition of $g(\omega)$ (2). However, we prefer the definition of $g(\omega)$ given here (2), because in this way the units of $g(\omega)$ are those of dipole moment squared multiplied by time.

[26]J. D. Poll and J. van Kranendonk, Can. J. Phys. 39, 189 (1961).

[27]J. D. Poll, J. L. Hunt, and J. W. MacTaggart, Can. J. Phys. 53, 954 (1975).

[28]M. Rotenberg, N. Metropolis, R. Birins, and J. K. Wooten, Jr., *The 3j and 6j Symbols* (The Technology Press, MIT, Cambridge, Mass., 1959).

[29]U. Fano, National Bureau of Standards, Washington, D.C., Report No. 1214, 1951 (unpublished).

[30]J. de Boer, Rep. Prog. Phys. 12, 305 (1949).

[31]G. Birnbaum and L. Frommhold (unpublished).

[32]C. Bottcher, A. Dalgarno, and E. L. Wright, Phys. Rev. A 7, 1606 (1973).

[33]G. Birnbaum, M. S. Brown, and L. Frommhold, Can. J. Phys. 59, 1544 (1982).
[34]L. Frommhold, Adv. Chem. Phys. 46, 1 (1981).
[35]W. Meyer, Chem. Phys. 17, 27 (1976).
[36]W. Kolos and L. Wolniewicz, J. Chem. Phys. 43, 2429 (1965).
[37]F. Mulder, A. van der Avoird, and P. E. S. Wormer, Mol. Phys. 37, 159 (1978).
[38]K. C. Ng, W. J. Meath, and A. R. Allnatt, Mol. Phys. 32, 177 (1976).
[39]A. R. W. McKellar, J. W. MacTaggart, and H. L. Welsh, Can. J. Phys. 53, 2026 (1975).
[40]C. S. Roberts, Phys. Rev. 131, 203 (1963).
[41]M. Krauss and F. H. Mies, J. Chem. Phys. 42, 2703 (1965).
[42]B. Tsapline and W. Kutzelnigg, Chem. Phys. Lett. 23, 173 (1973).
[43]A. W. Raczkowski and W. A. Lester, Jr., Chem. Phys. Lett. 47, 45 (1977).
[44]L. Zandee and J. Reuss, Chem. Phys. 26, 345 (1977).
[45]R. Ahlrichs, R. Penco, and G. Scoles, Chem. Phys. 19, 119 (1977).
[46]K. T. Tang and J. P. Toennies, J. Chem. Phys. 66, 1496 (1977).
[47]K. T. Tang and J. P. Toennies, J. Chem. Phys. 68, 5501 (1978).
[48]W. R. Rodwell and G. Scoles, J. Phys. Chem. 86, 1053 (1982).
[49]J. W. Riehl, J. L. Kinsey, J. S. Waugh, and J. H. Rugenheimer, J. Chem. Phys. 49, 5276 (1968).
[50]K. R. Foster and J. H. Rugenheimer, J. Chem. Phys. 56, 2632 (1972).
[51]I. Amdur and A. P. Malinauskas, J. Chem. Phys. 42, 3335 (1965).
[52]R. Shafer and R. G. Gordon, J. Chem. Phys. 58, 5422 (1973).
[53]One of the authors (L.F.) acknowledges valuable discussions with Professor W. Meyer on this point.
[54]G. Birnbaum and E. R. Cohen, Can. J. Phys. 54, 593 (1976).
[55]E. R. Cohen, L. Frommhold, and G. Birnbaum, J. Chem. Phys. 77, 4933 (1982).
[56]W. Meyer (private communication).
[57]A. M. Arthurs and A. Dalgarno, Proc. R. Soc. London, Ser. A 256, 540 (1960).
[58]H. B. Levine and G. Birnbaum, Phys. Rev. 154, 86 (1967).